AIAA JOURNAL
Vol. 47, No. 5, May 2009

Accuracy of Local and Nonlocal Linear Stability Theory in Swept Separation Bubbles

T. Hetsch*
Aircraft Research Association, Ltd., Bedford, England MK41 7PF, United Kingdom
and
U. Rist†
University of Stuttgart, D-70550 Stuttgart, Germany

DOI: 10.2514/1.37997

A series of swept laminar separation bubbles is used to investigate the principle applicability of the e^N method to laminar separation bubbles in swept configurations. To this end the effect of sweep and of the propagation direction of disturbance waves on the accuracy of linear stability theory and solutions of the parabolized stability equations is studied systematically. Direct comparisons of spatial linear stability theory and linear parabolized stability equation solutions to results of direct numerical simulations allow for a qualitative and quantitative evaluation of their performance in the presence of sweep, flow separation, and local backflow. A variety of Tollmien–Schlichting waves as well as the most amplified stationary crossflow vortex is analyzed within a sweep angle range between 0 and 45 deg. It turns out that even though linear stability theory works satisfactorily, parabolized stability equations are clearly preferable in terms of accuracy, especially for very oblique modes or larger sweep angles.

Nomenclature

A	=	amplitude distribution of a disturbance wave
Amp	=	local value of the amplification curve, maximal wave amplitude at given x position
L^*	=	reference length
N	=	N factor
Re	=	Reynolds number
U, u'	=	leading-edge normal velocity component of base flow and disturbances, respectively
V, v'	=	wall-normal velocity component of base flow and disturbances, respectively
W, w'	=	leading-edge parallel velocity component of base flow and disturbances, respectively
x, y, z	=	leading-edge normal, wall-normal, and leading-edge parallel coordinates
x_m	=	position of maximal DNS amplitude of mode in question
x_n	=	neutral point
x_{reatt}	=	reattachment position
x_{sep}	=	separation position
α_i	=	spatial amplification rate in chordwise direction
α_r	=	chordwise wave number
γ	=	spanwise wave number
Θ	=	phase of a disturbance wave
ν	=	kinematic viscosity
σ_i	=	chordwise wave number for PSE
σ_r	=	spatial amplification rate for PSE
Ψ	=	propagation direction of a boundary-layer disturbance
Ψ_∞	=	sweep angle
ω	=	angular frequency

Subscripts

e	=	quantity at upper domain edge
max	=	maximum value of a quantity
n	=	quantity at neutral point of a disturbance wave
s	=	quantity in streamline-orientated coordinate system
(ω/γ)	=	quantity of the mode with frequency ω and spanwise wave number γ
0	=	quantity at inflow
∞	=	quantity in potential freestream ahead of flat plate
*	=	special value of quantity

Superscripts

u	=	property of a quantity evaluated from the u-velocity component
*	=	dimensional quantity
ˆ	=	property of a Fourier mode

I. Introduction

MODERN variants of the e^N method based on linear stability theory (LST) still represent the most common tool for transition prediction in aircraft industry [1,2]. For such tasks it is possible to substitute LST by the linear parabolized stability equations (PSE), which essentially can be viewed as a consistent extension of the linear stability theory by nonlocal, nonparallel, and curvature effects. The application of PSE may lead to improved N-factor correlations [3], but the key question is whether possible gains in accuracy through PSE are significant enough to compete with the robustness and the user friendliness of a local LST analysis. The user must be aware that there is in principle an inherent step-size restriction for classical PSE and it additionally requires an initial condition for each mode due to its parabolic nature, which is often provided by LST. To address the potential step-size restriction, strategies have emerged in the past years to ease or remove them through modifications of the PSE equations. Employing them implies, on the other hand, accepting that a single or a few offending terms are neglected, whereas other terms of the same magnitude are contained. For details about the elliptical nature of this step-size restriction and suggestions how to overcome it the reader might want to refer to Herbert [4], Andersson et al. [5], Chang and Choudhari [6], or Li and Malik [7].

Received 10 April 2008; revision received 11 January 2009; accepted for publication 11 January 2009.

*Senior Project Scientist, Computational Aerodynamics Department, Manton Lane; thetsch@ara.co.uk.

†Professor, Institut für Aerodynamik und Gasdynamik, Pfaffenwaldring 21; rist@iag.uni-stuttgart.de.

A stability analysis of swept wings will frequently encounter swept separation bubbles. For instance, the flow phenomenon was detected on the slat of an Airbus A310 in landing configuration [8]. An application of the e^N method in such a context therefore depends on the ability of LST and PSE to model the propagation of low-amplitude disturbances in the vicinity of swept laminar separation bubbles realistically. Swept laminar separation bubbles represent a demanding base flow for both methods due to the presence of sweep, flow separation, and local backflow. The rapid growth of the boundary-layer thickness inside the bubble violates the parallel flow assumption of LST and might conflict with the PSE requirement of a slowly changing base flow in the streamwise direction. Note that the presence of a moderate backflow, on the other hand, does not inhibit an application of linear PSE: the disturbance waves, which PSE is solving for by means of a chordwise marching procedure, still propagate in that direction.

For the *unswept* case, both methods turned out to be applicable despite these difficulties. Marxen et al. [9] have successfully compared amplification curves and eigenfunctions based on LST to direct numerical simulation (DNS) results and laser Doppler anemometry measured profiles up to the middle of an investigated laminar separation bubble. Hein [10] applied PSE to the unswept version of the short separation bubble considered here and achieved excellent agreement for the growth rates of a two-dimensional Tollmien–Schlichting (TS) wave compared to DNS results by Rist and Maucher [11]. However, he noted "minor differences" upstream of the bubble and in its front part for oblique waves, which seem to increase with the wave angle.

Still unknown, on the other hand, is the general applicability and overall accuracy of LST and PSE in laminar separation bubbles in a swept, three-dimensional flow, where oblique modes and crossflow influences become increasingly important. To clarify this point in a systematic and quantitative manner the short laminar separation bubble of [11] has been extended to swept inflows [12,13]. A variation of the sweep angles $\Psi_\infty = 0$, 30, and 45 deg results in a series of laminar separation bubbles, which exhibit identical cross sections in agreement with the independence principle of incompressible flow in swept infinite geometries discussed in detail in [12]. $\Psi_\infty =$ 15 deg had been omitted as preliminary studies showed that the results would be very close to the unswept case. Thus, sweep angle effects are isolated and the linear disturbance amplification of low-amplitude Tollmien–Schlichting waves and crossflow vortices in this base flow can be determined by means of a subsequent unsteady DNS. Any difference of LST and PSE to this reference solution is entirely due to the inherent weaknesses of their modeling assumptions.

After a brief description of the numerical methods and the base flow in Sec. II the performances of LST and PSE are evaluated for Tollmien–Schlichting waves in Sec. III and for the linearly most amplified crossflow vortex in Sec. IV, followed by the conclusions in Sec. V.

II. Numerical Methods and Base Flow

The DNS calculations are split in a DNS of the steady laminar base flow and a succeeding DNS for the disturbance propagation. These DNS codes solve the three-dimensional Navier–Stokes equations for unsteady, incompressible flows in a vorticity–velocity formulation with a fourth- to sixth-order discretization. For an in-depth description of the DNS algorithms refer to Wassermann and Kloker [14]. LST results were gained from the same in-house code utilized in this reference. The PSE results were obtained by the code NOLOT of the DLR, German Aerospace Center, Göttingen, which was extensively validated [15]. A comprehensive overview over the PSE methodology is provided by Bertolotti et al. [16] and Herbert [17].

The most important base-flow parameters already described in [12,13] are repeated here as follows: All quantities in the paper are nondimensionalized by the chordwise reference length $L^* = 0.05$ m and the chordwise freestream velocity $U^*_\infty = 30$ m/s, which are held constant for all sweep angles. The x and z directions are taken normal and parallel to the leading edge with U and W being the associated base-flow velocity components, respectively. Periodicity is assumed in the spanwise direction only, resulting in a quasi-2-D base flow with $\partial/\partial z = 0$, but $W(x, y) \neq 0$. The calculation domain itself consists of an infinite flat plate subjected to an adverse pressure gradient caused by the deceleration of the chordwise potential flow velocity $U_e(x)$ shown in Fig. 1. Different sweep angles Ψ_∞ are realized by varying the spanwise freestream velocity $W_\infty = \tan(\Psi_\infty)$ and setting $W_e(x) = W_\infty$ at the upper domain boundary. At the inflow located at $x_0 = 0.37$, matching Falkner–Scan–Cooke [18] profiles are prescribed. With a kinematic viscosity of $\nu^* = 15 \times 10^{-6}$ m^2/s the flow can be characterized by $Re_{\delta 1} = U^*_\infty \cdot \delta_1(x_0)/\nu =$ 331, based on the displacement thickness at the inflow. In the chordwise direction the domain ends at $x = 5.05$, while the wall-normal coordinate y extends to $y = 0.06$ or 18 displacement thicknesses of the inflow profile.

The domain is resolved by 2786×193 grid points in x and y. This resolution stems from transitional scenarios concerning the interaction of Tollmien–Schlichting waves with swept laminar separation bubbles [19] and is more than sufficient for the purely linear disturbance amplification sought here. A typical oblique TS wave, for instance, is resolved with about 85 grid points per wavelength in x and the representation in span is exact due to the employed Fourier ansatz. A successful validation and a grid verification of the 45 deg separation bubble calculated on a grid with half the current resolution in x and y can be found in [12,13]. Thus, a family of swept laminar separation bubbles with laminar reattachment is obtained, which exhibit identical separation and reattachment positions at $x_{\text{sep}} = 1.75$ and $x_{\text{reatt}} = 2.13$ for arbitrary sweep angles. The base flow reaches its steady state, if the differences in all flow quantities of two consecutive pseudotime levels are smaller than 10^{-10}.

III. Linear Stability Theory and Parabolized Stability Equation Results for Tollmien–Schlichting Waves

In the following, the notation (ω/γ) is adopted for discrete modes in the frequency-spanwise wave-number spectrum. For the DNS-reference solution a packet of TS waves with varying spanwise wave numbers $\gamma\epsilon[-40, -30, -20, 0, 20, 30, 40]$ was excited in the disturbance strip displayed in Fig. 1a. Within, local periodic suction and blowing in the wall-normal direction through the surface allows

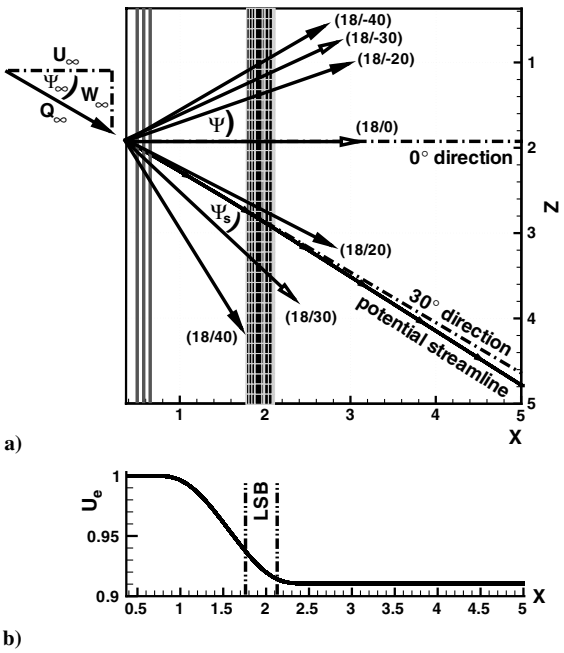

Fig. 1 Overview over 30 deg scenario: a) Top view with disturbance strip $x \in [0.5; 0.64]$, laminar separation bubble (LSB) between $x_{\text{sep}} = 1.75$ and $x_{\text{reatt}} = 2.13$, and potential streamline. b) Potential chordwise velocity U_e.

for the excitation of arbitrary two- or three-dimensional disturbance waves that are enforced with momentum input but no net mass flow [14]. The TS waves share the frequency $\omega = 18$ of the most amplified mode (18/0) of the 0-deg base flow. They are represented in Fig. 1a through arrows which indicate their propagation directions Ψ according to LST at $x = 1.4$. The angle Ψ_s expresses the same information in a streamline-orientated coordinate system. Small initial amplitudes of $A^u = 10^{-9}$ grant a purely linear development throughout the domain despite a considerable amplification of up to 4.5 orders of magnitude in the separated shear layer of the separation bubble.

Although the separation bubble is small, it has a noticeable effect on the overall flow stability as demonstrated by Fig. 2. It shows a direct comparison of a linear stability diagram for the 30 deg case with the attached flow obtained under the identical inflow conditions, but without the freestream deceleration. Amplification rates inside the separation bubble are up to 16 times higher, the frequency spectrum of amplified disturbances is significantly broader, and flow instability starts slightly earlier. The TS waves exhibit typical wavelengths between one-fourth to one-third of the separation bubble length $L_{\mathrm{LSB}} = 0.38$. The TS-wave packets were recomputed with LST and PSE to enable a quantitative comparison. This yields raw data in the form of amplification rates, wave numbers, and complex disturbance eigenmodes, which can be recast as wall-normal amplitude and phase distributions as in Fig. 3.

A. Postprocessing of the Raw Data for Direct Numerical Simulations, Parabolized Stability Equations, and Linear Stability Theory

After a transient phase the periodic disturbance excitation in combination with steady boundary conditions of the base flow leads

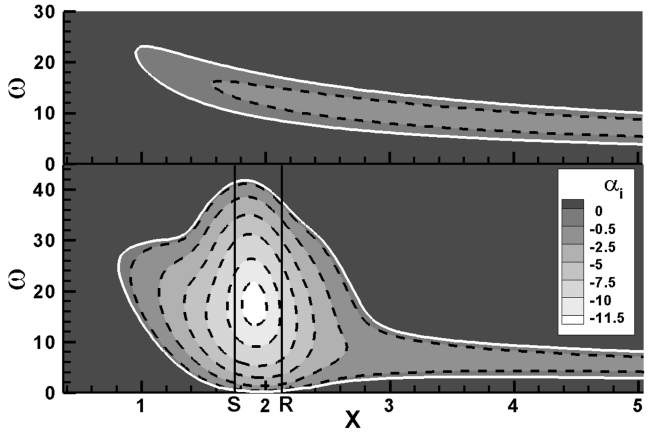

Fig. 2 Linear stability diagram (LST) for waves propagating normal to the leading edge ($\gamma = 0$): Comparison of 30-deg separation bubble with attached zero pressure gradient flow under identical inflow conditions. S = separation position; R = reattachment position.

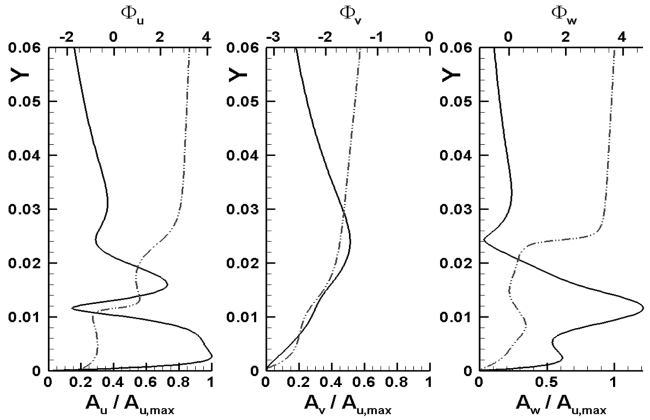

Fig. 3 PSE solution in the middle of the separation bubble at $x = 1.93$ in 45-deg base flow: wall-normal disturbance amplitude (solid lines) and phase (dash-dotted lines) distribution of TS mode (18/20).

to a time-periodic flowfield in the unsteady DNS. This enables a double Fourier analysis of the disturbance velocity component u' in time and span decomposing the flow into complex Fourier modes $\hat{u}_{(\omega/\gamma)}$ with phases $\hat{\Theta}_{(\omega/\gamma)}$ and amplitudes $\hat{A}_{(\omega/\gamma)}$. From them, DNS-amplification curves

$$\mathrm{Amp}_{\mathrm{DNS}}(x) = \max_{y}(\hat{A}_{(\omega/\gamma)}(x, y)) \tag{1}$$

as well as the local amplification rates $\alpha_{i,\mathrm{DNS}}$ and chordwise wave numbers $\alpha_{r,\mathrm{DNS}}$

$$\alpha_{i,\mathrm{DNS}} = -\frac{\partial(\ell_n(\mathrm{Amp}_{\mathrm{DNS}}))}{\partial x}, \qquad \alpha_{r,\mathrm{DNS}} = -\frac{\partial(\hat{\Theta})}{\partial x} \tag{2}$$

may be obtained. The general theoretical framework does not provide a preferred wall-normal distance y_* above the wall for the evaluation of the wave number $\alpha_{r,\mathrm{DNS}}$. Systematic comparisons with LST yielded that the dependency on y is only moderate so that the question is not decisive. The best agreement, however, was obtained in the potential freestream, for example, at $y_* = y_{\max}$ as done throughout this paper, with the first grid point above the wall being the second best choice. See Fasel and Konzelmann [20] for an in-depth discussion of this topic in two-dimensional boundary layers.

All PSE calculations were started from local solutions obtained from the built-in LST mode of NOLOT, which provide a complex eigenvalue–eigenvector pair in the form of the wave number α and a corresponding eigenvector of the local stream variables. In the absence of any upstream information additionally $\partial/\partial x = 0$ has to be assumed, effectively initializing the PSE process from a parallel flow during the startup phase. Afterward, the local disturbance wave properties α_r and α_i of the linear stability theory are corrected by the nonlocal streamwise influence of a slowly changing flowfield giving rise to the PSE-amplification rate σ_r and the corresponding chordwise wave number σ_i

$$\begin{aligned} \sigma_r &= -\alpha_i + \mathrm{Re}\left\{\frac{1}{\hat{u}} \cdot \frac{\partial \hat{u}}{\partial x}\right\} \\ \sigma_i &= \alpha_r + \mathrm{Im}\left\{\frac{1}{\hat{u}} \cdot \frac{\partial \hat{u}}{\partial x}\right\}, \quad \text{at } y_* = \{y_* | \hat{u}(y_*) = \max_{y \in [0, y_{\max}]} [\hat{u}(y)]\} \end{aligned} \tag{3}$$

For a quantitative comparison with the DNS these amplification rates are integrated to calculate the desired N factors, which describe the disturbance growth in the form of amplification curves $\mathrm{Amp}_{\mathrm{PSE}}$

$$N(x) = \int_{x_n}^{x} \sigma_r(\tilde{x}) \mathrm{d}\tilde{x}, \qquad \mathrm{Amp}_{\mathrm{PSE}}(x) = A_n e^{N(x)} \tag{4}$$

The same applies to the LST results, but due to its local character the equations simplify to

$$N(x) = \int_{x_n}^{x} -\alpha_i(\tilde{x}) \mathrm{d}\tilde{x}, \qquad \mathrm{Amp}_{\mathrm{LST}}(x) = A_n e^{N(x)} \tag{5}$$

Their free parameter, the initial amplitude A_n, is fitted to match the DNS results at the corresponding neutral point, which lies in the vicinity of $x_n = 0.95$ for the TS-wave package considered here. Figure 4a shows a direct comparison of the DNS, LST, and PSE-amplification curves based on Eqs. (1), (4), and (5) for the most oblique mode (18/40) of the highest sweep angle case. Clearly, LST is performing poorly for strongly oblique modes in contrast to the (18/20) in Fig. 4b, which is nearly aligned with the freestream of the 30 deg case. With an eye on its main industrial application, the e^N-based transition prediction, we can now systematically evaluate the accuracy of PSE as a function of the sweep angle and the propagation direction of the TS waves in the form of the relative amplitude error

$$r_a(x) = \frac{|\mathrm{Amp}_{\mathrm{DNS}}(x) - \mathrm{Amp}_{\mathrm{PSE}}(x)|}{|\mathrm{Amp}_{\mathrm{DNS}}(x)|} \tag{6}$$

at the point x_m, where the DNS solution peaks and can likewise proceed in a similar manner for LST. Despite its usefulness,

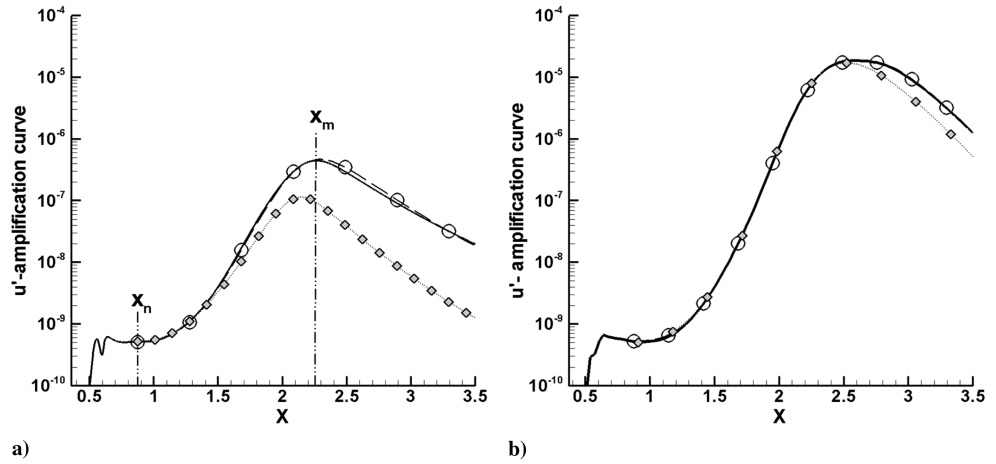

Fig. 4 Comparisons of DNS (solid lines), LST (lines with diamonds), and PSE (lines with circles) amplification curves with position of neutral point x_n and of maximal DNS amplitude x_m. a) Mode (18/40) for $\Psi = 45$ deg; b) mode (18/20) for $\Psi = 30$ deg.

however, Eq. (6) represents a point measurement and is as such unable to give any distributed information about the overall quality of both solutions within the bubble. Therefore, the $L2$ norm of these relative errors has been additionally evaluated at 12 preselected, equidistant locations starting from the separation and ending at the reattachment point

$$\|r_a\|_{L2} = \sqrt{(\sum_i r_a^2(x_i))} \tag{7}$$

All findings of Eqs. (6) and (7) were compiled into Tables 1 and 3, respectively. Table 2 provides the propagation direction of all modes at $x = 1.4$ in a body-fitted and streamline-orientated coordinate system based on LST, giving rise to the angles

$$\Psi = \arctan(\gamma/\alpha_r) \tag{8}$$

and Ψ_s as illustrated in Fig. 1a. This allows for the desired correlation of the amplitude error with the propagation direction. In the present base flow these angles change only moderately in the streamwise direction in the vicinity of the separation bubble, so that those values can be regarded as typical.

B. Effect of Sweep on the Accuracy of LST and PSE Results

As demonstrated by Table 1 and observable in Fig. 4a, the relative error of the LST-amplification curves is already quite high at the position of the maximal DNS amplitude. On the average it was found to be 40% for the 0-deg base flow and about 50% for the sweep angles $\Psi_\infty = 30$ deg and 45 deg. Overall, there is a tendency toward higher errors for increasing sweep angles Ψ_∞. Note that the 45 deg mode $(18/-40)$ exhibits an atypical behavior, as it is nearly neutrally stable. Table 3 shows that the error distribution through the bubble, measured in the L_2 norm, yields roughly the same trends. Technically, LST solutions could be obtained for the whole range of $\Psi_\infty \in [0, 45$ deg], although the oblique modes $(18/\pm 40)$ showed first, but still negligible convergence problems in their stable regions for $\Psi_\infty = 45$ deg. Attempts to proceed to higher sweep angles and to calculate a stability diagram for the 60-deg separation bubble with LST failed due to considerable problems with the eigenvalue search already in the unstable regions of the flowfield.

Table 1 Relative amplitude errors r_a (%) of Eq. (6) as a function of the TS wave (ω/γ) and sweep angle Ψ_∞. Left entry: LST with respect to DNS at peak x_m of DNS-amplification curve (see Fig. 4). Right entry: PSE

Ψ_∞	$r_a(18/-40)$	$r_a(18/-30)$	$r_a(18/-20)$	$r_a(18/0)$	$r_a(18/20)$	$r_a(18/30)$	$r_a(18/40)$	Mean, %
0 deg	58/8	55/6	16/5	16/4	16/5	55/6	58/8	39/6
30 deg	51/6	58/4	58/6	19/5	15/1	62/6	73/2	48/4
45 deg	25/6	51/2	59/2	19/5	39/9	81/10	78/11	50/6
Mean, %	45/7	55/4	44/4	18/5	23/5	66/7	70/7	46/6

Table 2 Propagation direction of evaluated TS waves (ω/γ) from Table 1 according to LST at $x = 1.4$. Left entry Ψ: leading-edge orientated coordinate system. Right entry Ψ_s: streamline orientated (see Fig. 1)

Ψ_∞	$\Psi(18/-40)$, deg	$\Psi(18/-30)$, deg	$\Psi(18/-20)$, deg	$\Psi(18/0)$, deg	$\Psi(18/20)$, deg	$\Psi(18/30)$, deg	$\Psi(18/40)$, deg
0 deg	$-41/-41$	$-32/-32$	$-22/-22$	0/0	22/22	32/32	41/41
30 deg	$-30/-61$	$-25/-56$	$-19/-49$	$0/-31$	$27/-4$	43/12	58/28
45 deg	$-25/-71$	$-22/-67$	$-17/-62$	$0/-46$	$32/-14$	54/8	79/33

Table 3 The norm $\|r_a\|_{L2}$ of relative amplitude errors within the bubble from Eq. (7) as a function of the analyzed TS wave (ω/γ) and sweep angle Ψ_∞. Left entry: LST with respect to DNS. Right entry: PSE

Ψ_∞	$r_a(18/-40)$	$r_a(18/-30)$	$r_a(18/-20)$	$r_a(18/0)$	$r_a(18/20)$	$r_a(18/30)$	$r_a(18/40)$	Mean
0 deg	0.55/0.39	0.26/0.23	0.17/0.15	0.30/0.08	0.17/0.15	0.26/0.23	0.55/0.39	0.32/0.23
30 deg	0.48/0.26	0.27/0.17	0.09/0.21	0.38/0.12	0.11/0.03	0.69/0.18	1.26/0.19	0.47/0.17
45 deg	0.64/0.23	0.37/0.13	0.13/0.10	0.37/0.14	0.25/0.18	1.51/0.24	2.07/0.11	0.76/0.16
Mean	0.55/0.29	0.30/0.18	0.13/0.15	0.35/0.11	0.18/0.12	0.82/0.22	1.30/0.23	0.52/0.19

PSE, on the other hand, is able to follow the DNS-reference solutions quite well through the long regions of pronounced growth in the separated shear layer. It predicts the total disturbance growth from the neutral point with a relative error of only 6% in the mean, nearly unaffected by the sweep angle. In the 45 deg case, beginning convergence problems made it necessary to double the step size for the modes (18/30) and (18/40). This coarse discretization led to higher errors compared to other PSE results.

C. Effect of the Propagation Direction on the Accuracy of LST and PSE Results

Table 2 demonstrates that the propagation direction Ψ grows monotonically with the spanwise wave number γ. For LST, the general trend, *larger errors for more oblique modes with larger* $|\gamma|$ *and therefore larger* $|\Psi|$, is much more pronounced than the effect of a rising sweep angle. The smallest relative errors between 15–19% are found for TS waves around $\gamma = 0$, which propagate broadly in the chordwise direction. For very oblique modes within the same base flows, the errors are up to 4 times higher. Note that there is no trend, *larger errors for modes with larger* $|\gamma_s|$, with respect to the direction of the potential streamline. PSE shows the same tendency of higher errors for more oblique modes, but much less pronounced than for LST. In the average the amplitude errors are 1.4 times higher than for two-dimensional waves.

D. Use of LST for the Calculation of Local Quantities

The high relative errors listed in Table 1 should not discourage the use of LST for oblique modes or swept flows in general. In all investigated cases LST systematically underpredicts the local DNS-amplification rates, as demonstrated for the 45 deg case in Figs. 5a and 5b for the modes (18/40) and (18/0) with the largest and the smallest relative errors in LST, respectively. Thus, fitting the amplification curves at the neutral point shows the *integrated* error from there up to the point of comparison. However, this is only necessary in the context of N-factor calculations.

For the direct results of LST, that is, local growth rates α_i and wave numbers α_r, only the error at the place of comparison has to be taken into account, which is significantly lower. For instance, Hein [10] has calculated the stability diagram for two-dimensional waves with PSE for the present 0-deg separation bubble and the recalculation of the diagram based on LST in Fig. 2 shows no discrepancy. Especially, the chordwise LST-wave number α_r shows a remarkable degree of accuracy throughout this study, largely independent of the sweep angle or the propagation direction of the analyzed mode. Even in the 45-deg base flow, where the greatest errors with respect to LST are to be expected, PSE fails to lead to any improvement over LST in that matter. This is demonstrated by the direct comparisons of the Ψ distributions in Fig. 5c, which stem from Eq. (8) and thus depend on α_r only. It also shows the moderate dependency of the propagation direction on x.

IV. LST and PSE Results for Stationary Crossflow Modes

In the 45-deg base flow the strength of the crossflow (CF) velocity W_s, the spanwise base-flow velocity in a streamline-orientated coordinate system, reaches a maximal value of about $W_{s,\max}/U_{s,e} = 9\%$ relative to the streamwise potential flow velocity $U_{s,e}$. As expected, the W_s profiles exhibit an inflection point indicating the influence of an inviscid crossflow instability. Systematic comparisons of LST results among stationary CF modes yielded maximal growth rates α_i of roughly one-third of those of the locally most amplified TS waves inside the separation bubble. The strongest

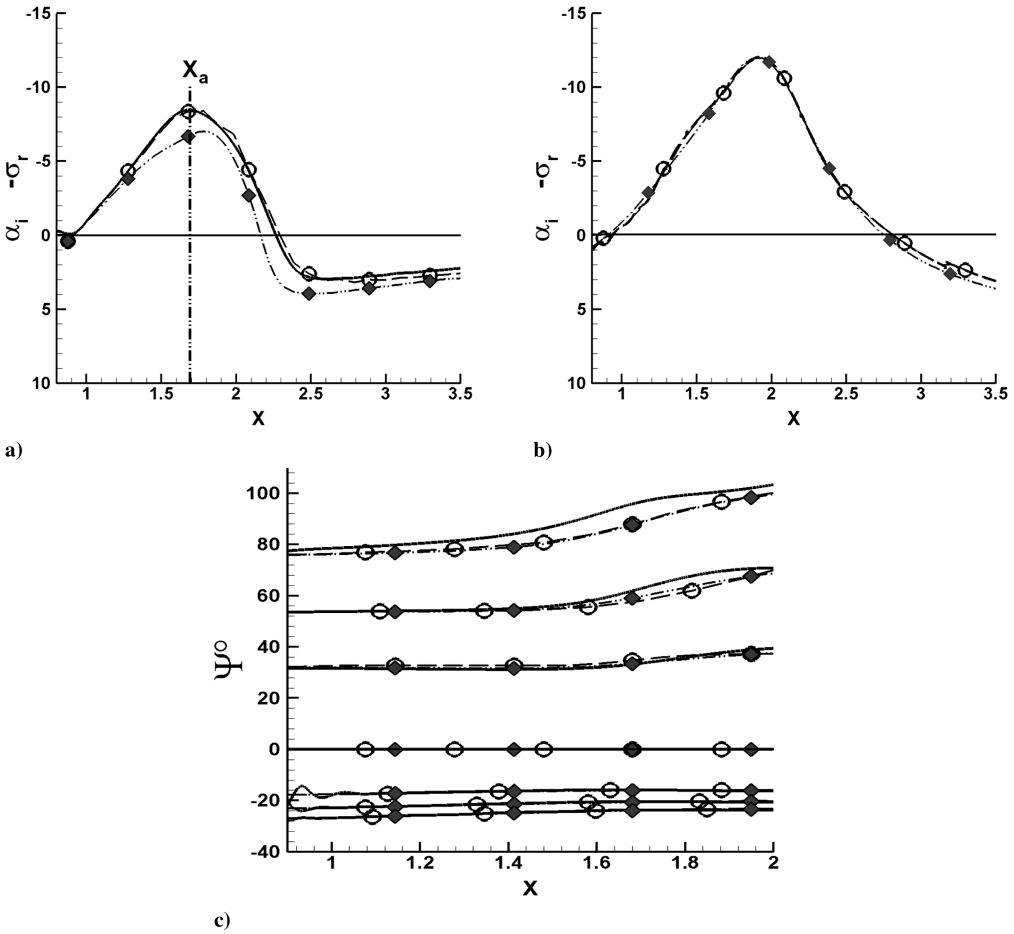

Fig. 5 Comparisons of local DNS (solid lines), LST (lines with diamonds), and PSE (lines with circles) results in the 45 deg case. Comparison of amplification rates from Eqs. (2) and (3): a) mode (18/40) with position of maximal DNS amplification x_a; b) mode (18/0); c) comparison of propagation direction Ψ for modes (18/γ) with $\gamma = -40, -30, -20, 0, 20, 30$, and 40 (from bottom to top), computed from local wave number α_r utilizing Eq. (8).

overall amplification is exhibited by the modes (0/40) and (0/50), which showed nearly identical amplification curves so that (0/40) was chosen for further comparison. Fitted to the neutral point at about $x_n = 1.35$ both linear theories follow the DNS result qualitatively well. Closer investigation, however, yields a specific problem with each of them.

LST, on the one hand, is not able to predict the actual form of the DNS curve anywhere, so that PSE solutions of CF vortices are preferable. This is obvious from Fig. 6a, where we fitted all LST- and PSE-amplification curves but one individually to the DNS result in order to compare the form of the amplification curves. After a transient phase PSE yields excellent agreement with the DNS solution, whereas LST shows only qualitative agreement. This is in accordance with the findings of Wassermann and Kloker [14], who examined several CF modes in an attached 45 deg boundary layer, which models a swept wing and showed that the LST systematically underpredicts the DNS-growth rates. In their study, amplification curves of DNS and LST differed at the middle of the domain already by a factor of 3 to 4. In the present base flow the local amplification rate α_i is in turn over- and underpredicted, but never coincides with the DNS in contrast to PSE as Fig. 6b shows. Nevertheless, for the chordwise wave number α_r LST is in very good agreement with DNS and no advantage can be gained through PSE as in the case of the TS waves.

PSE solutions of CF modes, on the other hand, depend on the position of their LST-initial condition to a certain degree as demonstrated by Fig. 6. Contrary to expectation, an early start upstream of the neutral point x_n yields worse results farther downstream, as the local PSE-amplification rates depart noticeably from the DNS solution during the first steps in the damped region, which unnecessarily prolongs the transient phase. This type of behavior might explain the minor differences especially in the upstream flow and front part of the separation bubble reported by Hein [10] as mentioned in the Introduction. The best agreement was obtained for starting positions x_{st} slightly downstream of the DNS-neutral point in the amplified region. This approach can be useful, if PSE results are used to identify the region of purely linear growth during the postprocessing of DNS data. In Fig. 6a this is demonstrated by the gray PSE curve with the open gradient symbols, which would confirm linear growth of the DNS solution throughout the investigated domain. Within the framework of transition prediction by linear methods with no DNS available, however, integration has to start at the neutral point itself leading to a prediction as exemplified by the black PSE curve with the filled circles, Fig. 6a. For the comparison with DNS, on the other hand, one should take the enlarged scale of Fig. 6a in comparison to previous plots of TS-amplification curves into account. To summarize, Fig. 6 emphasizes that LST-initial conditions are less suitable for CF modes, contrary to the behavior of TS waves up to moderate supersonic Mach numbers. Instead, alternative approaches such as the usage of multiscale solutions or nonparallel eigenvalue formulations should be considered, which have the potential to reduce such transient effects significantly [21].

V. Conclusions

The applicability and accuracy of linear stability theory and linear PSE was investigated for a generic series of short laminar separation bubbles with emphasis on their accuracy for oblique modes and the effect of sweep. LST and PSE were both found to be applicable in the whole sweep angle range of $\Psi_\infty = [0; 45\ \text{deg}]$.

A packet of TS waves with systematically varying spanwise wave number γ was quantitatively compared to DNS results for all sweep angles $\Psi_\infty = 0$, 30, and 45 deg. To mimic an e^N-type N-factor prediction, the amplification curves were fitted to the neutral point of the corresponding modes and the relative amplitude error at the position of the maximal DNS amplification were evaluated. In terms of accuracy, PSE is clearly superior to LST, which systematically underpredicts the DNS-growth rates. Averaged over all modes and sweep angles, the integrated error in the disturbance amplification was 6% for PSE compared to 46% for LST. Details can be found in Table 1. Note that an error of 64% already results in an amplitude factor difference of 2.8 between LST and DNS, which would correspond to an underprediction of LST by $\Delta N = 1$ in a N-factor prediction. On the other hand, the amplification in the separated shear layer is so strong compared to the attached boundary-layer flows—the maximum growth rate of the present laminar separation bubble is 16 times higher than that of the same inflow without pressure gradient—that even such an error would results in only a moderate Δx shift of the predicted transition location.

LST works best for the unswept case. The errors increase with a rising sweep angle, in the mean by a factor of 1.25 from $\Psi_\infty = 0$ deg to 45 deg. More pronounced is the dependency of LST from the propagation direction of the analyzed mode, which follows the general trend: *larger errors occur for modes with larger propagation angles*. In the present investigation the errors of the most oblique TS waves are up to 4 times higher than for two-dimensional waves. In application LST is very robust and easy to handle and automate because of its local character. It is well suited to obtain an overview, can be used for qualitative comparisons or predictions, and is especially useful when a great number of modes has to be calculated, as for stability diagrams. LST was remarkably accurate for the streamwise wave number α_r, for which no advantage could be gained through PSE. For the calculation of local wave properties based on α_r, such as the propagation direction, wave length, or phase speed, the use of LST can therefore be recommended even for very oblique modes in swept base flows.

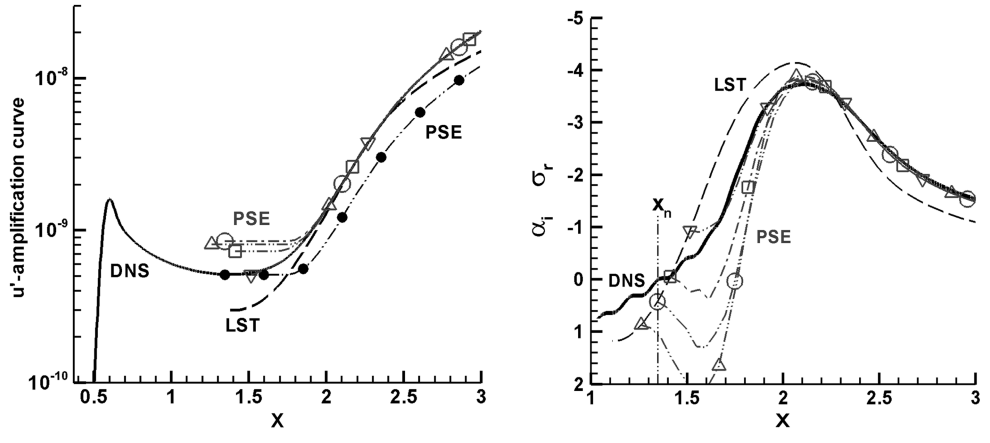

Fig. 6 Comparisons for steady CF vortex (0/40) with neutral point $x_n = 1.35$ in 45 deg base flow. DNS (solid lines), LST (dashed lines), PSE started from x_{st}: 1.26 (delta), 1.35 (circle), 1.41 (square), and 1.51 (gradient). In a) only: the filled circles indicate the PSE solution fitted to the neutral point, and otherwise the best fit of the curves to the DNS result. a) Comparison of amplification curves. b) Comparison of local amplification rates.

The accuracy of PSE results, on the other hand, is rather independent of the sweep angle, but the most oblique waves also showed increased errors. In the mean they differed from the minimum error of the mode $(18/-20)$ by a factor of 1.75. Because of its step-size restriction, traditional PSE as utilized here requires more attention per run. However, this issue can be addressed through modifications to the PSE equations, as discussed in the references cited in the Introduction. It is to be expected that this would have reduced the error for the 45 deg case further and the present case study illustrates that such an approach is generally desirable for high sweep angles and very oblique modes. PSE comes into play when greater accuracy is desired and is preferable for crossflow instabilities. Note that the present base flow was a flat-plate boundary layer. In curved geometries, PSE has the additional advantage of the inclusion of curvature terms. To summarize, the results show that *N*-factor prediction is in principle feasible in swept laminar separation bubbles, but should be based on PSE, if oblique TS waves or CF instabilities are expected to be dominant in the investigated transition scenario.

Acknowledgments

The financial support by the Deutsche Forschungsgemeinschaft (DFG) under contract number RI 680/12 is gratefully acknowledged. The authors would like to thank the DLR, German Aerospace Center —Göttingen and especially S. Hein for permission to use the linear NOLOT PSE code.

References

[1] Crouch, J. D., and Ng, L. L., "Variable *N*-Factor Method for Transition Prediction in Three-Dimensional Boundary Layers," *AIAA Journal*, Vol. 38, No. 2, 2000, pp. 211–216. doi:10.2514/2.973

[2] Schrauf, G., "Large-Scale Laminar-Flow Tests Evaluated with Linear Stability Theory," *Journal of Aircraft*, Vol. 41, No. 2, 2004, pp. 224–230. doi:10.2514/1.9280

[3] Schrauf, G., "Industrial View on Transition Prediction," *Recent Results in Laminar-Turbulent Transition—Selected Numerical and Experimental Contributions from the DFG-Verbundschwerpunktprogramm "Transition" in Germany*, edited by S. Wagner, M. Kloker, and U. Rist, Vol. 86, Notes on Numerical Fluid Mechanics, Springer, Berlin, 2003, pp. 111–122.

[4] Herbert, T., "Parabolized Stability Equations," AGARD TR 793, 1994, pp. 4-1–4-34.

[5] Andersson, J. P., Henningson, D. S., and Hanifi, A., "On a Stabilization Procedure for the Parabolic Stability Equations," *Journal of Engineering Mathematics*, Vol. 33, No. 3, 1998, pp. 311–332. doi:10.1023/A:1004367704897

[6] Chang, C.-L., and Choudhari, M., "Boundary-Layer Receptivity and Integrated Transition Prediction," AIAA Paper 2005-0526, 2005, p. 19.

[7] Li, F., and Malik, M. R., "On the Nature of PSE Approximation," *Theoretical and Computational Fluid Dynamics*, Vol. 8, 1996, pp. 253–273. doi:10.1007/BF00639695

[8] Greff, E., "In-Flight Measurements of Static Pressures and Boundary-Layer State with Integrated Sensors," *Journal of Aircraft*, Vol. 28, No. 5, 1991, pp. 289–299. doi:10.2514/3.46027

[9] Marxen, O., Lang, M., Rist, U., and Wagner, S., "A Combined Experimental/Numerical Study of Unsteady Phenomena in a Laminar Separation Bubble," *Flow, Turbulence and Combustion*, Vol. 71, Nos. 1–4, 2003, pp. 133–146. doi:10.1023/B:APPL.0000014928.69394.50

[10] Hein, S., "Linear and Nonlinear Nonlocal Instability Analyses for Two-Dimensional Laminar Separation Bubbles," *Proceedings of the IUTAM Symposium on Laminar-Turbulent Transition*, Springer, New York, 2000, pp. 681–686.

[11] Rist, U., and Maucher, U., "Direct Numerical Simulation of 2-D and 3-D Instability Waves in a Laminar Separation Bubble," *Application of Direct and Large Eddy Simulation to Transition and Turbulence*, AGARD CP-551, 1994, pp. 34-1–34-7.

[12] Hetsch, T., and U. Rist, "An Analysis of the Structure of Laminar Separation Bubbles in Swept Infinite Geometries," *European Journal of Mechanics B/Fluids* (submitted for publication).

[13] Hetsch, T., and Rist, U., "On the Structure and Stability of Three-Dimensional Laminar Separation Bubbles on a Swept Plate," *New Results in Numerical and Experimental Fluid Mechanics IV: Contributions to the 13. DGLR/STAB Symposium, 2002*, edited by C. Breitsamter, B. Laschka, H. J. Heinemann, and R. Hilbig, Vol. 87, Notes on Numerical Fluid Dynamics, Springer, Berlin, 2004, pp. 302–310.

[14] Wassermann, P., and Kloker, M., "Mechanisms and Passive Control of Crossflow-Vortex-Induced Transition in a Three-Dimensional Boundary Layer," *Journal of Fluid Mechanics*, Vol. 456, 2002, pp. 49–84. doi:10.1017/S0022112001007418

[15] Hein, S., Bertolotti, F. P., Simen, M., Hanifi, A., and Henningson, D., "Linear Nonlocal Instability Analysis, the Linear NOLOT Code," Institut für Strömungsmechanik, Göttingen, TR IB 223-94 A56, 1995.

[16] Bertolotti, F. P., Herbert, T., and Spalart, P. R., "Linear and Nonlinear Stability of the Blasius Boundary Layer" *Journal of Fluid Dynamics*, Vol. 242, 1992, pp. 441–474. doi:10.1017/S0022112092002453

[17] Herbert, T., "Parabolized Stability Equations," *Annual Review of Fluid Mechanics*, Vol. 29, Jan. 1997, pp. 245–283. doi:10.1146/annurev.fluid.29.1.245

[18] Cooke, J. J. C., "The Boundary Layer of a Class of Infinite Yawed Cylinders," *Proceedings of the Cambridge Philosophical Society (Mathematical and Physical Sciences)*, Vol. 46, 1950, pp. 645–648.

[19] Hetsch, T., and Rist, U., "The Effect of Sweep on Laminar Separation Bubble," *Sixth IUTAM Symposium on Laminar-Turbulent Transition, 2004*, edited by R. Govindarajan, Vol. 78, Fluid Mechanics and its Applications, Springer, Berlin, 2006, pp. 395–400.

[20] Fasel, H. F., and Konzelmann, U., "Non-Parallel Stability of a Flat-Plate Boundary Layer Using the Complete Navier-Stokes Equations," *Journal of Fluid Mechanics*, Vol. 221, No. 1, 1990, pp. 311–347. doi:10.1017/S0022112090003585

[21] Chang, C.-L., Malik, M. R., Erlebacher, G., and Hussaini, M. Y., "Compressible Stability of Growing Boundary Layers Using Parabolized Stability Equations," AIAA Paper 91-1636, 1991, p. 22.

A. Tumin
Associate Editor